Inorg. Chem. **2006**, *45*, 3895–3904

Structural and Photophysical Properties of Coordination Networks Combining $[Ru(Bpym)(CN)_4]^{2-}$ or $[\{Ru(CN)_4\}_2(\mu\text{-bpym})]^{4-}$ Anions (bpym = 2,2′-Bipyrimidine) with Lanthanide(III) Cations: Sensitized Near-Infrared Luminescence from Yb(III), Nd(III), and Er(III) Following Ru-to-Lanthanide Energy Transfer

Juan-Manuel Herrera,[†] Simon J. A. Pope,[‡] Harry Adams,[†] Stephen Faulkner,[‡] and Michael D. Ward*,[†]

Department of Chemistry, University of Sheffield, Sheffield S3 7HF, United Kingdom, and Department of Chemistry, University of Manchester, Oxford Road, Manchester M13 9PL, United Kingdom

Received December 19, 2005

Reaction of the cyanoruthenate anions $[Ru(bpym)(CN)_4]^{2-}$ and $[\{Ru(CN)_4\}_2(\mu\text{-bpym})]^{4-}$ (bpym = 2,2′-bipyrimidine) with lanthanide(III) salts resulted in the crystallization of coordination networks based on Ru–CN–Ln bridges. Four types of structure were obtained: $[Ru(bpym)(CN)_4][Ln(NO_3)(H_2O)_5]$ (**Ru**–**Ln**; Ln = Sm, Nd, and Gd) are one-dimensional helical chains; $[Ru(bpym)(CN)_4]_2[Ln(NO_3)(H_2O)_2][Ln(NO_3)_{0.5}(H_2O)_{5.5}](NO_3)_{0.5}\cdot 5.5H_2O$ (**Ru**–**Ln**; Ln = Er and Yb) are two-dimensional sheets containing cross-linked chains based on $Ru_2Ln_2(\mu\text{-CN})_4$ diamond units, which are linked into one-dimensional chains via shared Ru atoms; $[\{Ru(CN)_4\}_2(\mu\text{-bpym})][Ln(NO_3)(H_2O)_5]_2\cdot 3H_2O$ (**Ru$_2$**–**Ln**; Ln = Nd and Sm) are one-dimensional ladders with parallel Ln–NC–Ru–CN–Ln–NC strands connected by the bipyrimidine "cross pieces" acting as rungs on the ladder; and $[\{Ru(CN)_4\}_2(\mu\text{-bpym})][Ln(H_2O)_6]_{0.5}[Ln(H_2O)_4](NO_3)_{0.5}\cdot nH_2O$ (**Ru$_2$**–**Ln**; Ln = Eu, Gd, and Yb; n = 8.5, 8.5, and 8, respectively) are three-dimensional networks in which two-dimensional sheets of $Ru_2Ln_2(\mu\text{-CN})_4$ diamonds are connected via cyanide bridges to Ln(III) ions between the layers. Whereas **Ru**–**Gd** shows weak triplet metal-to-ligand charge-transfer (^{3}MLCT) luminescence in the solid state from the Ru-bipyrimidine chromophore, in **Ru**–**Nd**, **Ru**–**Er**, and **Ru**–**Yb**, the Ru-based emission is quenched, and all of these show, instead, sensitized lanthanide-based near-IR luminescence following a Ru → Ln energy transfer. Similarly, **Ru$_2$**–**Nd** and **Ru$_2$**–**Yb** show lanthanide-based near-IR emission following excitation of the Ru-bipyrimidine chromophore. Time-resolved luminescence measurements suggest that the Ru → Ln energy-transfer rate is faster (when Ln = Yb and Er) than in related complexes based on the $[Ru(bipy)(CN)_4]^{2-}$ chromophore, because the lower energy of the Ru-bpym ^{3}MLCT provides better spectroscopic overlap with the low-energy f–f states of Yb(III) and Er(III). In every case, the lanthanide-based luminescence is relatively short-lived as a result of the CN oscillations in the lattice.

Introduction

The use of cyanometalate anions as components of cyanide-bridged d−f coordination networks is appealing for many reasons. It is a synthetically straightforward way of combining d-block and f-block units without having to synthesize elaborate bridging ligands, and the short, conjugated bridging ligand affords relatively strong metal−metal interactions. For these reasons, cyanide-bridged d−f networks have been of particular recent interest for both their structural[1] and their magnetic[2] properties.

* Author to whom correspondence should be addressed. Tel.: 44 114-2229484. Fax: 44 114-2229346. E-mail: m.d.ward@sheffield.ac.uk.
[†] University of Sheffield.
[‡] University of Manchester.

(1) (a) Liu, S.; Meyers, E. A.; Shore, S. G. *Angew. Chem., Int. Ed.* **2002**, *41*, 3609. (b) Plecnik, C. E.; Liu, S.; Shore, S. G. *Acc. Chem. Res.* **2003**, *36*, 499 and refs therein. (c) Goubard, F.; Tabuteau, A. *Struct. Chem.* **2003**, *14*, 257. (d) Mullica, D. F.; Farmer, J. M.; Cunningham, B. P.; Kautz, J. A. *J. Coord. Chem.* **2000**, *49*, 239. (e) Kautz, J. A.; Mullica, D. F.; Cunningham, B. P.; Coombs, R. A.; Farmer, J. M. *J. Mol. Struct.* **2000**, *523*, 175. (f) Mullica, D. F.; Farmer, J. M.; Kautz, J. A. *Inorg. Chem. Commun.* **1999**, *2*, 73. (g) Miller, T. A.; Jeffery, J. C.; Ward, M. D. *CrystEngComm* **2003**, *5*, 495.

10.1021/ic0521574 CCC: $33.50
Published on Web 03/29/2006

The photophysical properties of such networks have, however, received much less attention. Examples of d → f energy transfer from dicyanoaurate and dicyanoargentate chromophores, resulting in sensitized lanthanide luminescence, have been reported by Patterson and co-workers;[3] Kunkely and Vogler showed how a heavy-atom effect of Gd(III) on hexacyanochromate(III) and hexacyanocobaltate(III) in solid-state materials results in strong phosphorescence from Cr-based or Co-based spin-forbidden d−d levels.[4] We have recently been investigating the structures and photophysical properties of coordination networks in which luminescent cyanometalate anions such as $[Ru(bipy)(CN)_4]^{2-}$ and its analogues are combined with lanthanide(III) cations.[5−7] In these networks, the presence of the diimine ligand means that the d-block anion has a long-lived, luminescent triplet metal-to-ligand charge-transfer (^{3}MLCT) state, which may be quenched by an energy transfer to the lanthanide, as long as the lanthanide ion has lower-lying f−f levels which can act as energy acceptors; this results in sensitized near-infrared (NIR) luminescence from Yb(III), Nd(III), Pr(III), and Er(III) following a Ru → lanthanide energy transfer across the Ru−CN−Ln linkages, whose rate varies according to the spectroscopic properties of the lanthanide concerned.[5] Such NIR emission from lanthanides has been of considerable recent interest because of its relevance to both biological imaging and telecommunications,[8] and several groups have demonstrated how d-block chromophores—with their intense and tunable absorption maxima in the visible region—can act as effective sensitizers of NIR luminescence from lanthanides in mixed-metal (d−f) complexes.[9]

In this paper, we report an extension of our recent work in this field and describe a structural and photophysical study of networks based on the cyanoruthenate complexes $[Ru(bpym)(CN)_4]^{2-}$ and $[\{Ru(CN)_4\}_2(\mu\text{-bpym})]^{4-}$ (bpym = 2,2′-bipyrimidine). Mononuclear $[Ru(bpym)(CN)_4]^{2-}$ has, in addition to the four cyanide groups as possible bridging ligands, an additional vacant site from the bipyrimidine ligand, which could also coordinate to lanthanide(III) cations; dinuclear $[\{Ru(CN)_4\}_2(\mu\text{-bpym})]^{4-}$ has eight cyanide groups available for coordination to lanthanides, which could result in networks displaying much higher connectivity. We therefore expect significantly different structural chemistry compared to earlier work using $[Ru(bipy)(CN)_4]^{2-}$.[5] Both complexes have absorptions in the visible region as a result of ^{1}MLCT transitions, which could result in them acting as visible-region absorbers which can sensitize low-energy NIR luminescence from appropriate lanthanide(III) centers. On the basis of the commonly observed pattern that the replacement of bipy with bpym results in a lowering of the MLCT levels,[9k] we also expect that the ability of the bpym-based complexes to act as energy donors to lanthanides will be altered both because of the different energy content of the ^{3}MLCT excited state and because of the consequent changes in donor−acceptor spectroscopic overlap with the lanthanides.

Results and Discussion

Synthesis and Crystallography. Reaction of bpym with 2 equivalents of $K_4[Ru(CN)_6]$ in aqueous HCl at reflux affords a mixture of mononuclear $[Ru(bpym)(CN)_4]^{2-}$ and dinuclear $[\{Ru(CN)_4\}_2(\mu\text{-bpym})]^{4-}$, which could be separated by ion-exchange chromatography and isolated as their potassium salts.[6,7]

Slow evaporation of aqueous solutions containing $K_2[Ru(bpym)(CN)_4]$ and $Ln(NO_3)_3{\cdot}6H_2O$ in a 1:5 molar ratio (Ln = Nd, Sm, Gd, Er, and Yb) afforded, in every case, a good crop of crystals. X-ray crystallographic (see Supporting Information) investigations showed that these were of two structural types, depending on the size of the lanthanide cation; in both cases, charge balance is provided by a $[Ru(bpym)(CN)_4]^{2-}/Ln^{3+}$/nitrate ratio of 1:1:1. For convenience, these complexes based on $[Ru(bpym)(CN)_4]^{2-}$ will be abbreviated where necessary as **Ru−Sm**, **Ru−Nd**, and so forth.

For the earlier lanthanides, $[Ru(bpym)(CN)_4][Ln(NO_3)(H_2O)_5]$ (Ln = Sm, Nd, and Gd) are isostructural with one another; the structure of $[Ru(bpym)(CN)_4][Nd(NO_3)(H_2O)_5]$ is shown in Figure 1. The complex forms a one-dimensional

(2) (a) Ma, B.-Q.; Gao, S.; Su, G.; Xu, G.-X. *Angew. Chem., Int. Ed.* **2001**, *40*, 434. (b) Figuerola, A.; Diaz, C.; Ribas, J.; Tangoulis, V.; Granell, J.; Lloret, F.; Mahia, J.; Maestro, M. *Inorg. Chem.* **2003**, *42*, 641. (c) Toma, L. M.; Delgado, F. S.; Ruiz-Pérez, C.; Carrasco, R.; Cano, J.; Lloret, F.; Julve, M. *Dalton Trans.* **2004**, 2836. (d) Herrera, J.-M.; Marvaud, V.; Verdaguer, M.; Marrot, J.; Kalisz, M.; Mathonière, C. *Angew. Chem., Int. Ed.* **2004**, *43*, 5468. (e) Figuerola, A.; Diaz, C.; El Fallah, M. S.; Ribas, J.; Maestro, M.; Mahia, J. *Chem. Commun.* **2001**, 1204. (f) Figuerola, A.; Ribas, J.; Casanova, D.; Maestro, M.; Alvarez, S.; Diaz, C. *Inorg. Chem.* **2005**, *44*, 6949.

(3) (a) Rawashdeh-Omary, M. A.; Larochelle, C. L.; Patterson, H. H. *Inorg. Chem.* **2000**, *39*, 4527. (b) Assefa, Z.; Shankle, G.; Patterson, H. H.; Reynolds, R. *Inorg. Chem.* **1994**, *33*, 2187.

(4) Kunkely, H.; Vogler, A. *Inorg. Chem. Commun.* **2004**, *7*, 770.

(5) (a) Davies, G. M.; Pope, S. J. A.; Adams, H.; Faulkner, S.; Ward, M. D. *Inorg. Chem.* **2005**, *44*, 4656. (b) Miller, T. A.; Jeffery, J. C.; Ward, M. D.; Adams, H.; Pope, S. J. A.; Faulkner, S. *Dalton Trans.* **2004**, 1524.

(6) Adams, H.; Alsindi, W.; Davies, G. M.; Duriska, M. B.; Easun, T. L.; Fenton, H.; Herrera, J.-M.; George, M. W.; Ronayne, K. L.; Sun, X.-Z.; Towrie, M.; Ward, M. D. *Dalton Trans.* **2006**, 39.

(7) Herrera, J.-M.; Baca, S. G.; Adams, H.; Ward, M. D. *Polyhedron* **2006**, *25*, 869.

(8) (a) Faulkner, S.; Matthews, J. L. In *Comprehensive Coordination Chemistry*, 2nd ed.; Ward, M. D., Ed.; Elsevier: Oxford, U. K., 2004; Vol. 9, p 913 and refs therein. (b) Motson, G. R.; Fleming, J. S.; Brooker, S. *Adv. Inorg. Chem.* **2004**, *55*, 361. (c) Tanabe, S. *C. R. Chim* **2002**, *5*, 815. (d) Kumar, G. A.; Riman, R.; Snitzer, E.; Ballato, J. *J. Appl. Phys.* **2004**, *95*, 40. (e) Bünzli, J.-C. G.; Piguet, C. *Chem. Soc. Rev.* **2005**, *34*, 1048.

(9) (a) Klink, S. I.; Keizer, H.; van Veggel, F. C. J. M. *Angew. Chem., Int. Ed.* **2000**, *39*, 4319. (b) Beeby, A.; Dickins, R. S.; FitzGerald, S.; Govenlock, L. J.; Maupin, C. L.; Parker, D.; Riehl, J. P.; Siligardi, G.; Williams, J. A. G. *Chem. Commun.* **2000**, 1183. (c) Imbert, D.; Cantuel, M.; Bünzli, J.-C. G.; Bernardinelli, G.; Piguet, C. *J. Am. Chem. Soc.* **2003**, *125*, 15698. (d) Torelli, S.; Imbert, D.; Cantuel, M.; Bernardinelli, G.; Delahaye, S.; Hauser, A.; Bünzli, J.-C. G.; Piguet, C. *Chem.—Eur. J.* **2005**, *11*, 3228. (e) Pope, S. J. A.; Coe, B. J.; Faulkner, S. *Chem. Commun.* **2004**, 1550. (f) Pope, S. J. A.; Coe, B. J.; Faulkner, S.; Bichenkova, E. V.; Yu, X.; Douglas, K. T. *J. Am. Chem. Soc.* **2004**, *126*, 9490. (g) Guo, D.; Duan, C.-Y.; Lu, F.; Hasegawa, Y.; Meng, Q.-J.; Yanagida, S. *Chem. Commun.* **2004**, 1486. (h) Glover, P. B.; Ashton, P. R.; Childs, L. J.; Rodger, A.; Kercher, M.; Williams, R. M.; De Cola, L.; Pikramenou, Z. *J. Am. Chem. Soc.* **2003**, *125*, 9918. (i) Shavaleev, N. M.; Moorcraft, L. P.; Pope, S. J. A.; Bell, Z, R.; Faulkner, S.; Ward, M. D. *Chem. Commun.* **2003**, 1134. (j) Shavaleev, N. M.; Moorcraft, L. P.; Pope, S. J. A.; Bell, Z, R.; Faulkner, S.; Ward, M. D. *Chem.—Eur. J.* **2003**, *9*, 5283. (k) Shavaleev, N. M.; Accorsi, G.; Virgili, D.; Bell, Z. R.; Lazarides, T.; Calogero, G.; Armaroli, N.; Ward, M. D. *Inorg. Chem.* **2005**, *44*, 61.

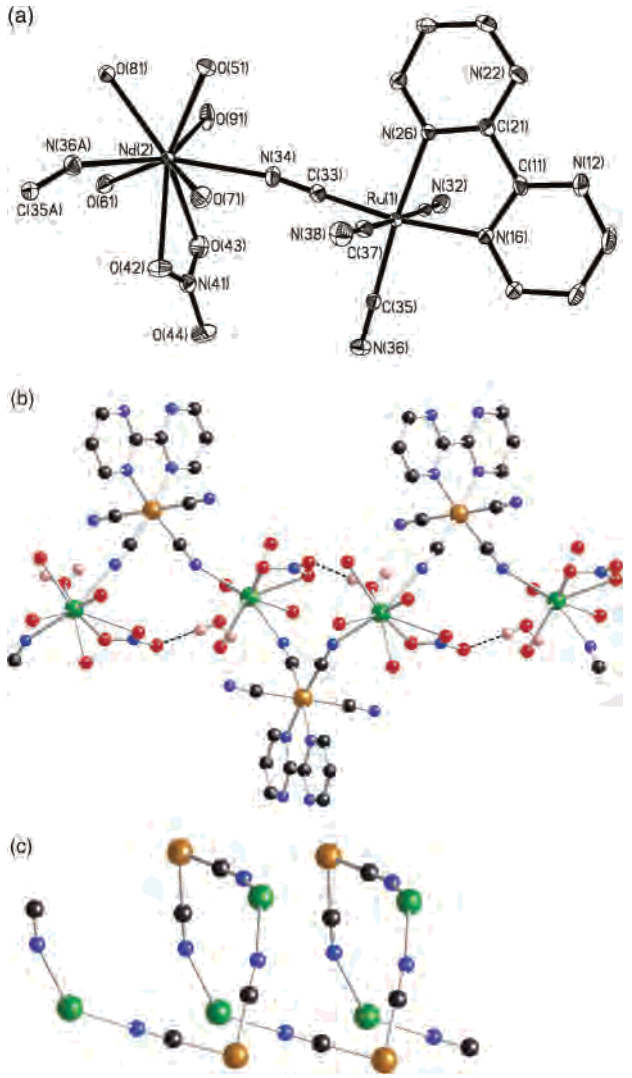

Figure 1. Crystal structure of $[Ru(bpym)(CN)_4][Nd(NO_3)(H_2O)_5]$. (a) An ORTEP view showing the asymmetric unit [with additional atoms from adjacent asymmetric units added to complete the coordination sphere around Nd(2)]. (b) A view of the chain structure (C, black; N, blue; Ru, brown; Nd, green; O, red; H, pink) with the OH···O hydrogen bonds between nitrate and water ligands on adjacent Nd centers shown as black dotted lines. (c) A stripped-down view emphasizing the helical disposition of the cyanide-bridged chain.

helical chain along the *c* axis, consisting of alternating $[Ru(bpym)(CN)_4]^{2-}$ and $[Nd(NO_3)(H_2O)_5]$ units linked by cyanide bridges, with the two cyanide ligands in the same plane as the bpym ligand of $[Ru(bpym)(CN)_4]^{2-}$ being those involved in the bridging interactions. The structural properties of the $[Ru(bpym)(CN)_4]^{2-}$ unit are unremarkable. The Nd(III) center is nine-coordinate, from five water ligands, the N-donor termini of two bridging cyanides, and a bidentate nitrate which is coordinated in a markedly asymmetric manner [Nd(1)−O(42), 2.515 Å; Nd(1)−O(43), 2.743 Å; difference between them $\Delta = 0.228$ Å]. The reason for the asymmetric coordination of the nitrate is not to relieve steric crowding—nine coordination for the large Nd(III) ion is not a problem—but to allow the "remote" oxygen atom of the nitrate, O(44), to participate in a hydrogen-bonding interaction with water ligand O(71) coordinated to the next Nd(III) center further along the chain [O(42)···O(71) separation, 2.718 Å]. The participation of the water molecule containing O(71) in hydrogen bonding results in the Nd(1)−O(71) bond (2.585 Å) being significantly longer than the other four Nd−O(water) bonds, which are all between 2.40 and 2.48 Å. It is clear that the formation of these OH···O hydrogen bonds, along the axis of the chain, is facilitated by the helical structure, which brings ligands attached to separate Nd(III) ions into close proximity. The pitch of the helical chain is just one unit cell length along the *c* axis, that is, 12.45 Å.

A comparison of this structure with that of the Gd(III) analogue is instructive, because Gd(III) is the smallest of the lanthanide(III) ions which give this structure. The gross structure is the same, but the smaller ionic radius of Gd(III) results in a more markedly asymmetric coordination of the nitrate ion, with Gd(1)−O(42) and Gd(1)−O(43) having distances of 2.462 and 2.893 Å, respectively ($\Delta = 0.431$ Å), such that the Gd(III) ion may now be considered as eight-coordinate with the nitrate monodentate. Again, the remaining nitrate oxygen atom O(44) engages in a hydrogen-bonding interaction with the water molecule O(71) of an adjacent Gd(III) center further along the chain; the O(44)···O(71) separation is 2.742 Å. As would be expected, the Sm(III) complex shows intermediate behavior, with the bond distances to the asymmetric nitrate being Sm(1)−O(41) = 2.495 Å and Sm(1)−O(42) = 2.763 Å ($\Delta = 0.268$ Å).

With the smaller lanthanide cations, a different structure $[Ru(bpym)(CN)_4]_2[Ln(NO_3)(H_2O)_2][Ln(NO_3)_{0.5}(H_2O)_{5.5}](NO_3)_{0.5}\cdot 5.5H_2O$ arises (Ln = Er and Yb). The structure of the Yb(III) complex **Ru−Yb** is shown in Figure 2. A complicated two-dimensional sheet network has formed, based on two crystallographically independent $[Ru(bpym)(CN)_4]^{2-}$ units and two crystallographically independent Yb(III) centers. In contrast to the previous structure, one $[Ru(bpym)(CN)_4]^{2-}$ unit [containing Ru(1)] is connected to four Yb(III) centers, using all four cyanides as bridging ligands. The other $[Ru(bpym)(CN)_4]^{2-}$ unit [containing Ru(2)] is, however, only connected to two Yb(III) centers, using the two cyanides in the same plane as the bpym ligand for the bridging interactions; the two axial cyanides are involved in CN···HOH hydrogen-bonding interactions with water ligands from nearby Yb(III) centers. The structure consists of $Ru_2Yb_2(\mu\text{-}CN)_4$ diamond units, which are linked into one-dimensional chains via shared Ru atoms. One such set of 1-D chains propagates along the *y* axis and contains alternating Ru(1)/Yb(1) and Ru(1)/Yb(2) groupings in alternate diamonds; the second set of 1-D chains propagates along the *z* axis and contains alternating Ru(2)/Yb(2) and Ru(1)/Yb(2) squares. The two sets of chains are joined by the Ru(1)/Yb(2) centers which are common to both. In Figure 2b, these two chains are shown with red and blue bonds (*y* and *z* axis, respectively), with the intersection between them being shown with purple bonds. Yb(2) is accordingly coordinated by four cyanide ligands from four different $[Ru(bpym)(CN)_4]^{2-}$ units [two Ru(1) and two Ru(2) units], and its 8-fold coordination is completed by two water ligands and a bidentate nitrate. Yb(1), in contrast, has only two cyanide ligands [from Ru(1) units], and its coordination

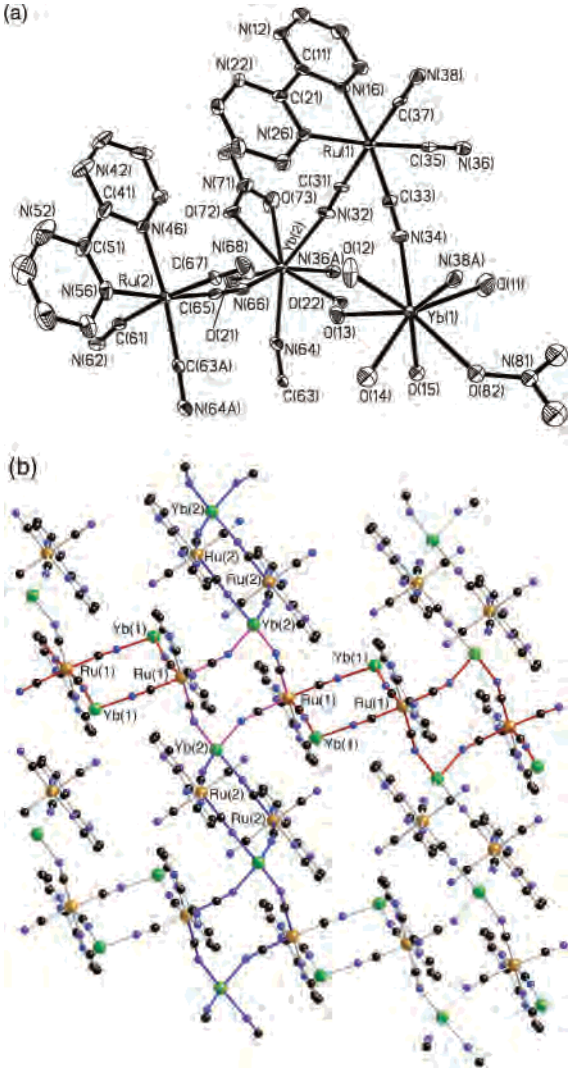

Figure 2. Crystal structure of $[Ru(bpym)(CN)_4]_2[Yb(NO_3)(H_2O)_2]$ $[Yb(NO_3)_{0.5}(H_2O)_{5.5}](NO_3)_{0.5}\cdot 5.5H_2O$. (a) An ORTEP view showing the asymmetric unit of the network [with additional atoms from adjacent asymmetric units added to complete the coordination sphere around Yb(1), Yb(2), and Ru(2); lattice water molecular omitted for clarity]. Only one component of the disorder involving the nitrate ligand N(81)/O(82)/O(83)/O(84) (50% occupancy) and the water ligand O(82W) [which occupies the same site as O(82)] is shown. (b) A view emphasizing the cross-linked array of $Ru_2(\mu\text{-}CN)_4Yb_2$ diamonds (C, black; N, blue; Ru, brown; Yb, green). Orthogonal chains are highlighted with red and blue bonds, with the intersection between them colored with purple bonds. Water ligands on the Yb atoms are omitted for clarity.

sphere also contains five water molecules [two of which, O(14) and O(15), are disordered over two closely spaced sites]. The 8-fold coordination around Yb(1) is completed by O(82), which belongs to a water molecule (50% of the time) or a monodentate nitrate (50% of the time); charge balance is completed by an uncoordinated nitrate ion in the lattice, which also has a site occupancy of 50%. **Ru−Er** is isostructural to **Ru−Yb**.

Slow evaporation of aqueous solutions containing $K_4[\{Ru(CN)_4\}_2(\mu\text{-bpym})]$ and 8 equivalents of $Ln(NO_3)_3\cdot 6H_2O$ (Ln = Nd, Sm, Eu, Gd, and Yb) afforded crops of dark-red crystalline product in good yield. Again, two distinct structural types of coordination network appear, depending on the size of the lanthanide cation: $[\{Ru(CN)_4\}_2(\mu\text{-bpym})]$-

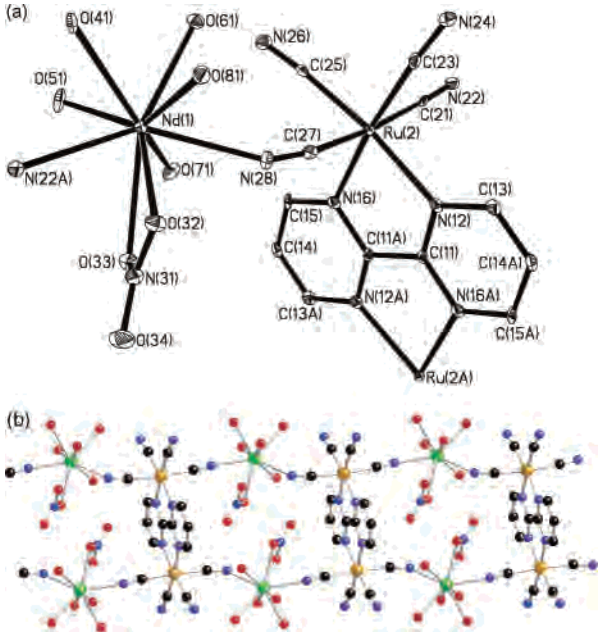

Figure 3. Crystal structure of $[\{Ru(CN)_4\}_2(\mu\text{-bpym})][Nd(NO_3)(H_2O)_5]_2\cdot 3H_2O$. (a) An ORTEP view showing the asymmetric unit (with additional atoms from adjacent asymmetric units added to complete the bipyrimidine ligand); lattice water molecules are omitted for clarity. (b) A view showing the one-dimensional ladder structure (C, black; N, blue; Ru, brown; Nd, green; O, red).

$[Ln(NO_3)(H_2O)_5]_2$ is formed with the earlier lanthanides (Ln = Nd and Sm) and $[\{Ru(CN)_4\}_2(\mu\text{-bpym})][Ln(H_2O)_6]_{0.5}[Ln^{III}(H_2O)_4](NO_3)_{0.5}$ is formed with later lanthanides from Eu onward (Ln = Eu, Gd, and Yb). In the former cases, the ratio of $\{Ru(CN)_4\}^{2-}/Ln^{3+}$/nitrate is 2:2:2 in the asymmetric unit; in the latter, the proportions are 2:1.5:0.5. This series of complexes, based on $[\{Ru(CN)_4\}_2(\mu\text{-bpym})]^{4-}$, will be abbreviated where necessary as **Ru_2−Eu** and so forth.

The structure of $[\{Ru(CN)_4\}_2(\mu\text{-bpym})][Nd(NO_3)(H_2O)_5]_2\cdot 3H_2O$ (**Ru_2−Nd**) is shown in Figure 3 and is a one-dimensional ladder with parallel Nd−NC−Ru−CN−Nd−NC strands connected by the bipyrimidine "cross pieces" acting as rungs on the ladder, linking the Ru centers of adjacent strands. In this structure, it is the axial pair of cyanide ligands at each Ru center which act as bridging ligands to propagate the chain. Adjacent ladders are connected by hydrogen-bonding interactions involving water ligands in one ladder and (equatorial) cyanides in the next, with the N(21)···O(41) interladder separation being 2.82 Å. There are also hydrogen-bonding interactions between the two strands of one ladder, involving O(34) of the nitrate ligand and O(71) on the adjacent strand (separation 2.87 Å). The Nd(III) centers are nine-coordinate, from two cyanide ligands, five water ligands, and a bidentate nitrate. The Sm(III) analogue **Ru_2−Sm** is isostructural.

The structure of $[\{Ru(CN)_4\}_2(\mu\text{-bpym})][Eu(H_2O)_6]_{0.5}[Eu(H_2O)_4](NO_3)_{0.5}$ (**Ru_2−Eu**) is shown in Figure 4; it has a complex three-dimensional network consisting of two-dimensional sheets which are stacked on top of each other and held together by additional bridging cyanide interactions. Figure 4b shows a view looking along the *b* axis, which

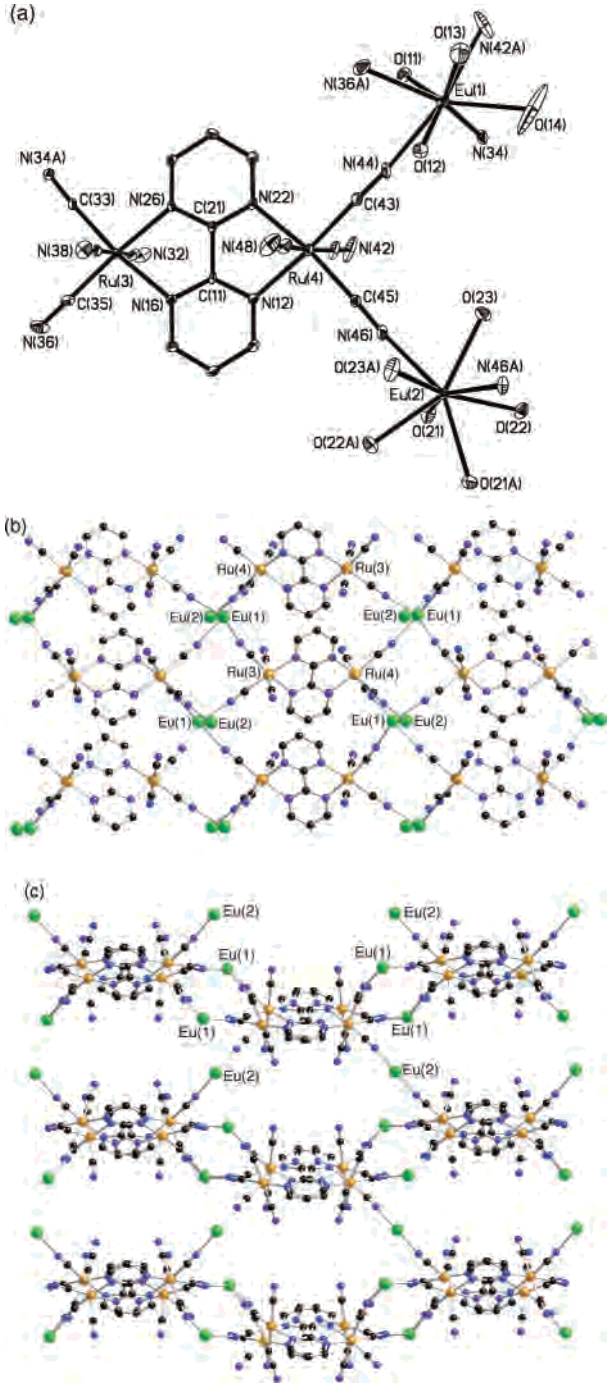

Figure 4. Crystal structure of $[\{Ru(CN)_4\}_2(\mu\text{-bpym})][Eu(H_2O)_6]_{0.5}[Eu(H_2O)_4](NO_3)_{0.5}\cdot 8.5H_2O$. (a) An ORTEP view showing the asymmetric unit [with additional atoms from adjacent asymmetric units added to complete the coordination sphere around Eu(1), Eu(2), and Ru(3)]; lattice water molecules are omitted for clarity. (b) A view along the crystallographic *b* axis of a two-dimensional layer, with water ligands on the Eu atoms omitted for clarity. (c) A view along the crystallographic *c* axis, showing how the two-dimensional layers depicted in the previous view are connected by Eu(2) ions, which are cyanide-bridged to the layers above and below. Water ligands are omitted for clarity.

shows a cyanide-bridged two-dimensional sheet in the *ac* plane, in which it is clear that the $[\{Ru(CN)_4\}_2(\mu\text{-bpym})]^{4-}$ units and the lanthanide cations are arranged in rows, with a sequence of $Ru_2Eu_2(\mu\text{-CN})_4$ diamonds [containing Eu(1) only] oriented along the *c* axis. Figure 4c shows a view along the *c* axis, looking at these sheets edge-on, which shows how the sheets shown in Figure 4b are held together by a layer of Eu(2) centers, with each Eu(2) being coordinated by one cyanide from the sheet above and one from the sheet below. Thus, each Eu(1), within a sheet, is eight-coordinate from four bridging cyanide ligands and four water ligands [one of which, O(12), is disordered over two sites], and each Eu(2), between the sheets, is also eight-coordinate from two cyanide and six water ligands. Five of the eight cyanide ligands in each $[\{Ru(CN)_4\}_2(\mu\text{-bpym})]^{4-}$ unit are involved in direct bridging to lanthanide cations. The complexes with the smaller lanthanides are isostructural, apart from small changes in the coordination number around the lanthanide; in $[\{Ru(CN)_4\}_2(\mu\text{-bpym})][Yb(H_2O)_6]_{0.5}[Yb(H_2O)_4](NO_3)_{0.5}$, for example, Yb(1) is seven-coordinate, from four cyanide ligands and three water ligands (two of which are disordered over two sites each); Yb(2) remains eight-coordinate [like Eu(2)] from two cyanide and six water ligands.

Photophysical Properties. In aqueous solution, $K_2[Ru(bpym)(CN)_4]$ shows ^{1}MLCT absorption maxima at 342 and 437 nm and is orange;[6] $K_4[\{Ru(CN)_4\}_2(\mu\text{-bpym})]$ shows ^{1}MLCT absorption maxima at 362 and 510 nm and is deep red.[7] The lower energy of the ^{1}MLCT transitions in the dinuclear complex compared to that of the mononuclear one is a typical pattern and is due to a lowering in energy of the π^* orbitals of bpym on coordination of the second electropositive metal ion. Neither complex shows any significant luminescent emission from a fluid solution, in contrast to the "parent" complex $[Ru(bipy)(CN)_4]^{2-}$, presumably because of the lower energy of the ^{3}MLCT state, which allows easier nonradiative decay via vibrational pathways. We have shown, however, using transient IR spectroscopic measurements, that the ^{3}MLCT lifetimes of $K_2[Ru(bpym)(CN)_4]$ and $K_4[\{Ru(CN)_4\}_2(\mu\text{-bpym})]$ in D_2O are 3.4 ns and ~1 ns, respectively.[6,10]

For the solid-state samples, we examined first the photophysical properties of **Ru**−**Gd** and **Ru$_2$**−**Gd** as controls because, in these cases, there is no possibility of a Ru → Gd energy transfer because of the high (UV region) energy of the lowest excited state of Gd(III), so the inherent photophysical properties of the cyanoruthenate chromophores in these crystalline environments will, therefore, be apparent. For **Ru**−**Gd**, excitation at 337 nm generated a broad, weak luminescence peak centered at 640 nm, ascribable to ^{3}MLCT emission from the $[Ru(bpym)(CN)_4]^{2-}$ unit. From the onset of the high-energy end of the spectrum (580 nm), we can estimate the ^{3}MLCT energy as ~17 000 cm^{-1}. The luminescence decay fit reasonably well to a single-exponential decay with $\tau = 80$ ns. This is considerably longer than the lifetime we observed in solution, which is a consequence of the interaction of the cyanide ligands with highly electropositive Gd(III) centers, an effect which increases the energy of the ^{3}MLCT state and, therefore, also increases the emission lifetime.[5,11] In contrast, we could not detect luminescence from **Ru$_2$**−**Gd**, presumably a consequence of its much lower

(10) Easun, T.; Herrera, J.-M.; Alsindi, W.; George, M. W.; Ward, M. D. Unpublished results.
(11) Ward, M. D. *Coord. Chem. Rev.* In press.

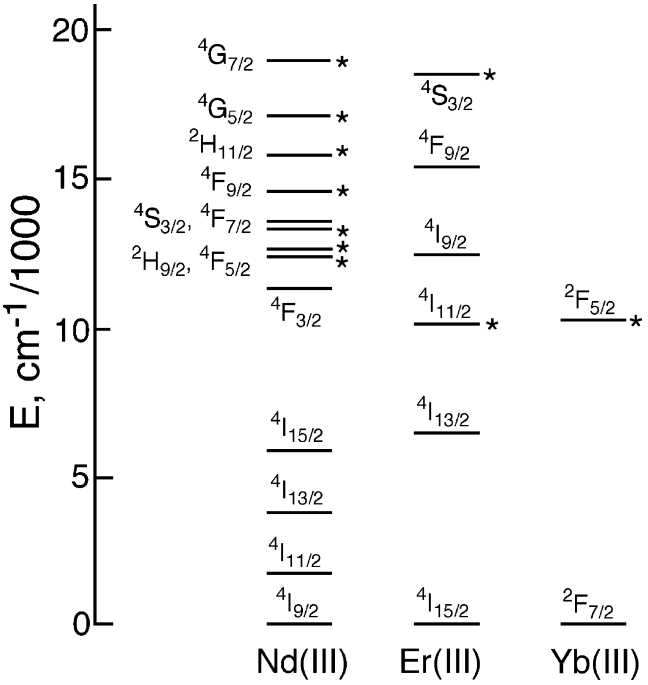

Figure 5. Lowest f−f energy levels of the lanthanide(III) ions discussed in this paper. The levels labeled * are those which can act as energy acceptors by either Förster or Dexter mechanisms according to the selection rules given in the main text.

MLCT excited-state energies and, hence, shorter lifetime (as in solution).

We then examined the NIR emission from the five complexes **Ru**−**Ln** (Ln = Nd, Er, and Yb) and **Ru$_2$**−**Ln** (Ln = Nd and Yb) as microcrystalline powders; in these complexes, the lanthanide is a potential near-IR emitter with low-energy f−f levels, which can be sensitized by an energy transfer from the Ru-based chromophore. A diagram of the relevant lanthanide-based energy levels is in Figure 5. All of the crystalline samples used for luminescence studies were grown from D_2O rather than H_2O to minimize the deleterious effects of O−H oscillators on the lanthanide emission.[12] In every case, the Ru-based MLCT emission was absent, indicative of quenching by an energy transfer to the lanthanide from which we would expect to see sensitized emission. In all of the complexes investigated, excitation into the UV absorption manifold of the Ru-bipyrimidine unit at either 337 or 430 nm resulted in sensitized NIR luminescence from the lanthanide at its characteristic wavelengths (Yb, 980 nm; Nd, 1060 and 1340 nm; and Er, 1530 nm), which can only have occurred following a Ru → Ln photoinduced energy transfer in each case. The lifetimes of these are collected in Table 1, and representative time-resolved emission spectra are in Figure 6. As we have pointed out before for luminescence on powdered solid samples,[5] we do not expect the "clean" single-exponential decay kinetics that are characteristic of luminescence in solution, because (i) the emitting lanthanide centers are not necessarily all in the same crystallographic environment and (ii) crystalline particles are necessarily heterogeneous, with molecules at the surface or at defect sites being in a different environment from those in the bulk. The lifetimes quoted in Table 1 are those derived from the best fit of the luminescence decay data to a single-exponential (in four cases) or dual-exponential (in one case) decay and are subject to a higher uncertainty than would be the case for solution data, but the fits are still reasonable.

It is immediately clear that (i) an energy transfer from the Ru-bipyrimidine chromophores to give sensitized NIR emission from the lanthanides can be confirmed in all five cases and (ii) the luminescence lifetimes of the lanthanides are short, as we have noted before in cyanide-based coordination networks.[5] These points will be discussed in turn. The occurrence of a Ru → Ln energy transfer in the **Ru**−**Ln** series, signaled by the appearance of sensitized emissions for all three complexes (Ln = Nd, Er, and Yb), means that the energy transfer is fast compared to the lifetime of the ^{3}MLCT state of the Ru-bpym chromophore (~80 ns); that is, $k_{EnT} > 1.2 \times 10^7$ s^{-1} in all three cases. In fact, given the complete quenching of the Ru-based emission, this is a lower limit, and assuming that we would be able to detect residual Ru-based emissions with a lifetime of 10 ns, we can estimate that $k_{EnT} >$ ca. 10^8 s^{-1} in all three cases.

Table 1. Luminescence Lifetimes of the Solid-State Materials[a]

complex	τ/ns	complex	τ/ns
Ru−**Gd**	80[b]	**Ru**−**Nd**	64[c]
Ru−**Yb**	587[c]	**Ru**−**Er**	43, 300[c,d]
Ru$_2$−**Yb**	245[c]	**Ru$_2$**−**Nd**	66[c]

[a] Measured at room temperature using either 337 or 430 nm excitation. [b] Ru-based emission; lifetime measured at 700 nm. [c] Lanthanide-based emission; lifetime measured at 980 nm (Yb), 1055 and 1340 nm (Nd), and 1530 nm (Er). [d] Er-based emission clearly fit better to a biexponential decay than a monoexponential decay.

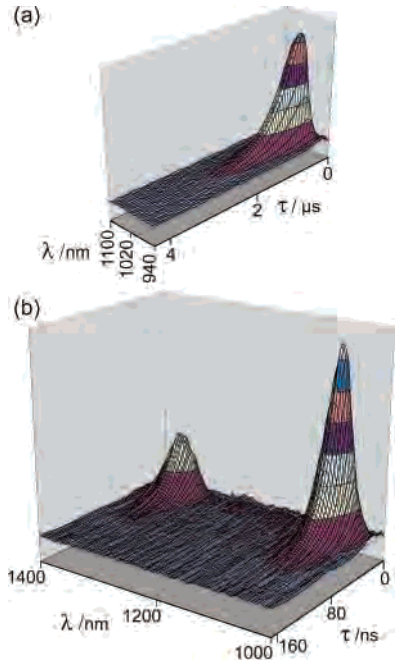

Figure 6. Time-resolved emission spectra for (a) **Ru**−**Yb** and (b) **Ru**−**Nd** showing the sensitized lanthanide-based luminescence following energy transfer from the Ru-based chromophore after excitation at 337 nm. Lifetimes (Table 1) are obtained by deconvoluting these traces from the detector response function.

(12) Beeby, A.; Clarkson, I. M.; Dickins, R. S.; Faulkner, S.; Parker, D.; Royle, L.; de Sousa, A. S.; Williams, J. A. G.; Woods, M. *J. Chem. Soc., Perkin Trans. 2* **1999**, 493.

Table 2. Analytical and IR Spectroscopic Data for the New Complexes

complex	elemental analysis (%C, %H, %N)[a]	principal IR spectral peaks, cm^{-1}[b]
$[Ru(bpym)(CN)_4][Nd(NO_3)(H_2O)_5]$	21.7 (21.9), 2.1 (2.4), 18.8 (19.1)	3435, 2111, 2079, 2070, 2039, 1618, 1384
$[Ru(bpym)(CN)_4][Sm(NO_3)(H_2O)_5]$	21.4 (21.6), 2.1 (2.4), 18.8 (18.9)	3430, 2112, 2079, 2072, 2043, 1619, 1384
$[Ru(bpym)(CN)_4][Gd(NO_3)(H_2O)_5]$	21.5 (21.4), 1.9 (2.4), 18.6 (18.7)	3434, 2112, 2079, 2073, 2047, 1623, 1400
$[Ru(bpym)(CN)_4]_2[Er(NO_3)(H_2O)_2][Er(NO_3)_{0.5}(H_2O)_{5.5}](NO_3)_{0.5}\cdot 5.5H_2O$	19.9 (20.3), 2.2 (2.7), 17.5 (17.8)	3428, 2136, 2100, 2066, 1633, 1384
$[Ru(bpym)(CN)_4]_2[Yb(NO_3)(H_2O)_2][Yb(NO_3)_{0.5}(H_2O)_{5.5}](NO_3)_{0.5}\cdot 5.5H_2O$	20.4 (20.1), 2.2 (2.6), 17.5 (17.6)	3413, 2140, 2105, 2066, 1634, 1384
$[\{Ru(CN)_4\}_2(\mu\text{-bpym})]\text{-}[Nd(NO_3)(H_2O)_5]_2\cdot 3H_2O$	15.7 (15.8), 2.3 (2.6), 15.5 (16.1)	3413, 2115, 2076, 2063, 2046, 1616, 1406, 1384
$[\{Ru(CN)_4\}_2(\mu\text{-bpym})]\text{-}[Nd(NO_3)(H_2O)_5]_2\cdot 3H_2O$	15.5 (15.7), 2.2 (2.6), 15.9 (16.0)	3436, 2115, 2079, 2050, 1626, 1400, 1384
$[\{Ru(CN)_4\}_2(\mu\text{-bpym})][Eu(H_2O)_6]_{0.5}[Eu(H_2O)_4](NO_3)_{0.5}\cdot 8.5H_2O$	17.0 (17.4), 3.1 (3.4), 15.4 (15.8)	3431, 2115, 2072, 1627, 1408, 1384
$[\{Ru(CN)_4\}_2(\mu\text{-bpym})][Gd(H_2O)_6]_{0.5}[Gd(H_2O)_4](NO_3)_{0.5}\cdot 8.5H_2O$	16.8 (17.2), 3.1 (3.3), 15.6 (15.7)	3424, 2116, 2076, 1635, 1408, 1384
$[\{Ru(CN)_4\}_2(\mu\text{-bpym})][Yb(H_2O)_6]_{0.5}[Yb(H_2O)_4](NO_3)_{0.5}\cdot 8H_2O$	17.2 (17.0), 2.8 (3.2), 15.5 (15.5)	3421, 2123, 2077, 1622, 1408, 1384

[a] Calculated figures are in parentheses. [b] Recorded on the pure crystalline solids using an ATR accessory. The set of up to four peaks between 2000 and 2150 cm^{-1} arises from the cyanide vibrations.

Table 3. Summary of Crystal, Data Collection, and Refinement Details

complex	$[Ru(bpym)(CN)_4][Nd(NO_3)(H_2O)_5]$	$[Ru(bpym)(CN)_4][Sm(NO_3)(H_2O)_5]$
formula	$C_{12}H_{16}N_9NdO_8Ru$	$C_{12}H_{16}N_9O_8RuSm$
mol wt	659.65	665.76
T, K	150(2)	150(2)
cryst syst	orthorhombic	orthorhombic
space group	*Pna*2(1)	*Pna*2(1)
a, Å	24.791(2)	24.791(2)
b, Å	6.5425(6)	6.5425(6)
c, Å	12.4486(12)	12.4486(12)
α,deg	90	90
β,deg	90	90
γ,deg	90	90
V, $Å^3$	2019.1(3)	2019.1(3)
Z	4	4
ρ, g cm^{-3}	2.170	2.190
cryst size, mm^3	0.35 × 0.28 × 0.07	0.29 × 0.16 × 0.07
μ, mm^{-1}	3.353	3.690
data, restraints, parameters	4719, 16, 281	4617, 16, 281
final *R*1, *wR*2	0.0209, 0.0458	0.0243, 0.0519

complex	$[Ru(bpym)(CN)_4][Gd(NO_3)(H_2O)_5]$	$[Ru(bpym)(CN)_4]_2[Er(NO_3)(H_2O)_2]$-$[Er(NO_3)_{0.5}(H_2O)_{5.5}](NO_3)_{0.5}\cdot 5.5H_2O$
formula	$C_{12}H_{16}GdN_9O_8Ru$	$C_{24}H_{38}Er_2N_{18}O_{19}Ru_2$
mol wt	672.66	1419.38
T, K	150(2)	150(2)
cryst syst	orthorhombic	triclinic
space group	*Pna*2(1)	$P\bar{1}$
a, Å	24.713(4)	12.3927(15)
b, Å	6.5565(10)	13.2752(16)
c, Å	12.5558(19)	14.3563(18)
α,deg	90	81.027(2)
β,deg	90	77.828(2)
γ,deg	90	89.565(2)
V, $Å^3$	2034.4(5)	2279.7(5)
Z	4	2
ρ, g cm^{-3}	2.196	2.068
cryst size, mm^3	0.29 × 0.16 × 0.08	0.38 × 0.23 × 0.07
μ, mm^{-1}	4.035	4.382
data, restraints, parameters	4644, 16, 281	10236, 18, 561
final *R*1, *wR*2	0.0276, 0.0526	0.0446, 0.1155

complex	$[Ru(bpym)(CN)_4]_2[Yb(NO_3)(H_2O)_2]$-$[Yb(NO_3)_{0.5}(H_2O)_{5.5}](NO_3)_{0.5}\cdot 5.5H_2O$	$[\{Ru(CN)_4\}_2(\mu\text{-bpym})]$-$[Nd(NO_3)(H_2O)_5]_2\cdot 3H_2O$
formula	$C_{24}H_{38}N_{18}O_{19}Ru_2Yb_2$	$C_{16}H_{32}N_{14}Nd_2O_{19}Ru_2$
mol wt	1430.94	1215.18
T, K	150(2)	100(2)
cryst syst	triclinic	monoclinic
space group	$P\bar{1}$	*C*2/*c*
a, Å	12.3768(11)	20.352(4)
b, Å	13.1438(12)	6.4118(13)
c, Å	14.3078(13)	28.182(6)
α,deg	81.532(2)	90
β,deg	77.860(2)	107.95(3)
γ,deg	89.426(2)	90
V, $Å^3$	2250.2(4)	3498.6(12)
Z	2	4
ρ, g cm^{-3}	2.112	2.307
cryst size, mm^3	0.32 × 0.23 × 0.07	0.40 × 0.20 × 0.07
μ, mm^{-1}	4.866	3.862
data, restraints, parameters	10086, 18, 561	4020, 0, 240
final *R*1, *wR*2	0.0436, 0.1133	0.0295, 0.0870

Table 3 (Continued)

complex	$[\{Ru(CN)_4\}_2(\mu\text{-bpym})]$-$[Sm(NO_3)(H_2O)_5]_2 \cdot 3H_2O$	$[\{Ru(CN)_4\}_2(\mu\text{-bpym})][Eu(H_2O)_6]_{0.5}$-$[Eu(H_2O)_4](NO_3)_{0.5} \cdot 8.5H_2O$
formula	$C_{16}H_{32}N_{14}O_{19}Ru_2Sm_2$	$C_{16}H_{37}Eu_{1.5}N_{12.5}O_{17}Ru_2$
mol wt	1227.40	1106.66
T, K	150(2)	120(2)
cryst syst	monoclinic	orthorhombic
space group	*C*2/*c*	*Aba*2
a, Å	20.268(13)	25.160(5)
b, Å	6.393(4)	22.200(4)
c, Å	28.096(18)	13.623(3)
α,deg	90	90
β,deg	107.944(11)	90
γ,deg	90	90
V, Å^3	3464(4)	4609(3)
Z	4	8
ρ, g cm^{-3}	2.354	1.932
cryst size, mm^3	0.30 × 0.08 × 0.05	0.16 × 0.14 × 0.02
μ, mm^{-1}	4.293	3.300
data, restraints, parameters	3951, 15, 240	8708, 8, 446
final *R*1, *wR*2	0.0321, 0.0779	0.0305, 0.0868

complex	$[\{Ru(CN)_4\}_2(\mu\text{-bpym})][Gd(H_2O)_6]_{0.5}$-$[Gd(H_2O)_4](NO_3)_{0.5} \cdot 8.5H_2O$	$[\{Ru(CN)_4\}_2(\mu\text{-bpym})][Yb(H_2O)_6]_{0.5}$–$[Yb(H_2O)_4](NO_3)_{0.5} \cdot 8H_2O$
formula	$C_{16}H_{37}Gd_{1.5}N_{12.5}O_{17}Ru_2$	$C_{16}H_{36}N_{12.5}O_{16.5}Ru_2Yb_{1.5}$
mol wt	1114.60	1129.27
T, K	150(2)	150(2)
cryst syst	orthorhombic	orthorhombic
space group	*Aba*2	*Aba*2
a, Å	25.1267(14)	24.9856(6)
b, Å	22.1514(11)	21.9719(5)
c, Å	13.6062(11)	13.4830(3)
α,deg	90	90
β,deg	90	90
γ,deg	90	90
V, Å^3	7573.1(8)	7401.9(3)
Z	8	8
ρ, g cm^{-3}	1.955	2.027
cryst size, mm^3	0.17 × 0.09 × 0.03	0.24 × 0.05 × 0.02
μ, mm^{-1}	3.458	4.639
data, restraints, parameters	12848, 8, 445	11074, 8, 440
final *R*1, *wR*2	0.0377, 0.0951	0.0291, 0.0705

In the $[Ru(bipy)(CN)_4]^{2-}/Ln^{3+}$ systems we described recently,[5] the k_{EnT} values for the Ru → Ln energy transfer were estimated to be 3×10^6 s^{-1} (Ru → Yb), 1×10^7 s^{-1} (Ru → Er), and 2×10^8 s^{-1} (Ru → Nd). Thus, the Ru → Yb energy transfer from $[Ru(bpym)(CN)_4]^{2-}$ in **Ru−Yb** must therefore be at least a factor of 30 faster than it was from $[Ru(bipy)(CN)_4]^{2-}$ across the same distance, and we cannot detect a grow-in for the Yb-centered luminescence, in contrast to what we observed for $[Ru(bipy)(CN)_4]^{2-}$.[5] The most likely explanation for this is the lower energy of the $[Ru(bpym)(CN)_4]^{2-}$ ^{3}MLCT level compared to that of $[Ru(bipy)(CN)_4]^{2-}$ (∼17 000 cm^{-1} instead of 20 000 cm^{-1} in the crystalline solids), which will result in a better spectroscopic overlap of the tail of the energy-donor triplet state with the energy-accepting f−f level of Yb(III) at 980 nm.

Similar reasoning can be applied to the Ru → Er energy transfer. The f−f levels of Er(III) that are most likely to overlap with the ^{3}MLCT state of $[Ru(bpym)(CN)_4]^{2-}$ are (in order of increasing energy) $^4I_{11/2}$, $^4I_{9/2}$, and $^4F_{9/2}$, which lie between 10 000 and 16 000 cm^{-1} above the $^4I_{15/2}$ ground state. Taking the selection rules for Förster ($|\Delta J| = 2$, 4, and 6) and Dexter energy transfers ($\Delta J = 0$ and ±1) into account,[13] we see that excitation from the ground state of Er(III) to the $^4I_{9/2}$ and $^4F_{9/2}$ states by an energy transfer is formally forbidden ($\Delta J = 3$, disallowed by both mechanisms), which means that the $^4I_{11/2}$ level at ∼10 000 cm^{-1} is the best energy acceptor. This is similar to the situation for Yb(III): a single energy-accepting f−f state at a low energy will give a better spectroscopic overlap with the d-block energy donor as the ^{3}MLCT level of $[Ru(bpym)(CN)_4]^{2-}$ is itself lowered in energy. Consequently, we see a faster Ru → Er energy transfer from $[Ru(bpym)(CN)_4]^{2-}$, by 1 order of magnitude, than we did from $[Ru(bipy)(CN)_4]^{2-}$. For **Ru−Nd**, as with $[Ru(bipy)(CN)_4]^{2-}/Nd^{3+}$, Nd(III) has a high density of f−f states of the appropriate energy such that the energy transfer is expected to be fast.[5]

The particularly short luminescence lifetimes of the lanthanide centers are noteworthy. Luminescence lifetimes for coordinatively saturated Yb(III), Nd(III), and Er(III) complexes are commonly on the order of microseconds, typically > 10 *μ*s for Yb(III), 1 *μ*s for Nd(III), and 2 *μ*s for Er(III),[9] or more if there are no high-energy oscillators close to the metal center.[14] In solid-state materials such as oxides or fluorides, luminescence lifetimes can be very long

(13) de Sá, G. F.; Malta, O. L.; de Mello Donegá, C.; Simas, A. M.; Longo, R. L.; Santa-Cruz, P. A.; da Silva, E. F. *Coord. Chem. Rev.* **2000**, *196*, 165.

(14) Basset, A. P.; van Deun, R.; Nockemann, P.; Glover, P. B.; Kariuki, B. M.; van Hecke, K.; van Meervely, L.; Pikramenou, Z. *Inorg. Chem.* **2005**, *44*, 6140.

Table 4. Selected Bond Distances for the Structures $[Ru(bpym)(CN)_4][Ln(NO_3)(H_2O)_5]$

	Ln = Nd	Ln = Sm	Ln = Gd
Ru(1)−C(33)	1.958(4)	1.968(5)	1.971(5)
Ru(1)−C(35)	1.971(4)	1.980(5)	1.993(5)
Ru(1)−C(31)	2.028(4)	2.043(5)	2.057(6)
Ru(1)−C(37)	2.042(4)	2.043(5)	2.053(6)
Ru(1)−N(26)	2.101(3)	2.113(4)	2.122(5)
Ru(1)−N(16)	2.110(3)	2.116(4)	2.122(4)
Ln(2)−O(61)	2.403(3)	2.383(3)	2.364(4)
Ln(2)−O(91)	2.436(3)	2.424(3)	2.398(4)
Ln(2)−O(81)	2.472(3)	2.449(3)	2.436(4)
Ln(2)−O(51)	2.480(3)	2.449(3)	2.417(4)
Ln(2)−N(34)	2.479(3)	2.463(4)	2.443(5)
Ln(2)−O(42)	2.515(3)	2.495(3)	2.462(4)
Ln(2)−N(36A)	2.540(3)	2.513(4)	2.485(5)
Ln(2)−O(71)	2.585(3)	2.578(3)	2.553(4)
Ln(2)−O(43)	2.743(3)	2.763(4)	2.893(5)

(millisecond time scale) even for NIR emitters, because the heavy atoms in the lattice mean that all vibrational modes are very low in energy and, therefore, are poor energy acceptors.[15] In our coordination networks, however, the observed lifetimes are approximately 1 order of magnitude shorter than those in molecular complexes and many orders of magnitude less than those in oxide/fluoride crystals. We ascribe this to the presence of the relatively high-energy C−N oscillators at ∼2000 cm^{-1}, which are directly coordinated to the lanthanide centers. The energy of the cyanide vibrations is actually comparable to that of O−D vibrations, and of course, deuterated solvents such as D_2O and MeOD are routinely used in lanthanide chemistry as *poor* energy acceptors (at least, poor compared to O−H).[16] However, the cross-linked cyanide-bridged network appears to provide a mechanism for the rapid dispersal of phonons through the lattice, making the cyanide ligands in the solid much more effective quenchers than O−D oscillators of comparable frequency in molecular species.

All of the above comments apply to the series **Ru_2−Ln** also. The dinuclear chromophore $[\{Ru(CN)_4\}_2(\mu\text{-bpym})]^{4-}$ is not luminescent in either aqueous solutions or the solid state, but clearly (on the basis of its absorption spectrum), its ^{3}MLCT energy must be significantly lower than that of $[Ru(bpym)(CN)_4]^{2-}$ and therefore, must be an even better match for the energy-accepting $^2F_{5/2}$ level of Yb(III) at 10 200 cm^{-1}. The Ru → Yb energy transfer is therefore expected to be faster in **Ru_2−Yb** than in **Ru−Yb**; similarly, although we cannot quantify it in this case because we do not know the lifetime of the energy donor $[\{Ru(CN)_4\}_2(\mu\text{-bpym})]^{4-}$ unit, it must be fast enough to compete with the intrinsic deactivation of the ^{3}MLCT state of the $[\{Ru(CN)_4\}_2(\mu\text{-bpym})]^{4-}$ unit. The same is also true of the Ru → Nd energy transfer in **Ru_2−Nd**. The emission lifetimes from Yb(III) and Nd(III) in these complexes are, again, short and comparable to those observed in the **Ru−Ln** series (Table 1).

(15) (a) Kassab, L. R. P.; Fukumoto, M. E.; Cacho, V. D. D.; Setter, N. U.; Morimoto, N. I. *Opt. Mater.* **2005**, *27*, 1576. (b) Filippov, V. V.; Pershukevich, P. P.; Kuznetsova, V. V.; Homenko, V. S. *J. Lumin.* **2002**, *99*, 185. (c) Cascales, C.; Zaldo, C.; Sáez-Puche, R. *Chem. Mater.* **2005**, *17*, 2052. (d) Philipps, J. F.; Töpfer, T.; Ebendorff-Heidepriem, H.; Ehrt, D.; Sauerbrey, R. *Appl. Phys. B* **2001**, *72*, 399.

(16) Horrocks, W. D.; Sudnick, D. R. *Acc. Chem. Res.* **1981**, *14*, 384.

Table 5. Selected Bond Distances for the Structures $[Ru(bpym)(CN)_4]_2[Ln(NO_3)(H_2O)_2][Ln(NO_3)_{0.5}(H_2O)_{5.5}](NO_3)_{0.5}\cdot 5.5H_2O$

	Ln = Er	Ln = Yb
Ru(1)−C(35)	1.960(8)	1.962(8)
Ru(1)−C(33)	1.966(8)	1.976(7)
Ru(1)−C(31)	2.024(8)	2.022(7)
Ru(1)−C(37)	2.033(8)	2.026(7)
Ru(1)−N(16)	2.110(6)	2.107(6)
Ru(1)−N(26)	2.111(6)	2.103(6)
Ru(2)−C(63C)	1.959(7)	1.946(7)
Ru(2)−C(65)	1.975(8)	1.976(7)
Ru(2)−C(67)	2.036(8)	2.031(8)
Ru(2)−C(61)	2.044(8)	2.034(8)
Ru(2)−N(46)	2.119(6)	2.105(6)
Ru(2)−N(56)	2.121(6)	2.112(6)
Ln(1)−O(11)	2.378(6)	2.367(6)
Ln(1)−O(12)	2.369(6)	2.357(6)
Ln(1)−O(13)	2.353(5)	2.329(5)
Ln(1)−O(14)	2.406(10)	2.363(9)
Ln(1)−O(14′)	2.276(17)	2.37(2)
Ln(1)−O(15)	2.360(16)	2.255(15)
Ln(1)−O(15′)	2.343(9)	2.344(9)
Ln(1)−N(34)	2.349(6)	2.320(6)
Ln(1)−N(38A)	2.352(7)	2.318(7)
Ln(1)−O(82)	2.426(5)	2.430(5)
Ln(2)−O(21)	2.318(6)	2.312(6)
Ln(2)−N(36B)	2.349(7)	2.313(6)
Ln(2)−N(32)	2.375(7)	2.351(6)
Ln(2)−N(66)	2.383(7)	2.353(6)
Ln(2)−O(22)	2.389(5)	2.382(5)
Ln(2)−O(72)	2.391(6)	2.355(5)
Ln(2)−N(64)	2.397(6)	2.366(6)
Ln(2)−O(73)	2.496(6)	2.498(6)
Ln(2)−N(71)	2.863(7)	2.842(8)

Table 6. Selected Bond Distances for the Structures $[\{Ru(CN)_4\}_2(\mu\text{-bpym})][Ln(NO_3)(H_2O)_5]_2\cdot 3H_2O$

	Ln = Nd	Ln = Sm
Ru(2)−C(23)	1.979(6)	1.990(5)
Ru(2)−C(25)	1.999(5)	1.979(5)
Ru(2)−C(27)	2.024(6)	2.034(5)
Ru(2)−C(21)	2.041(5)	2.023(5)
Ru(2)−N(16)	2.119(5)	2.116(4)
Ru(2)−N(12)	2.140(5)	2.127(4)
Ln(1)−O(41)	2.458(4)	2.418(4)
Ln(1)−O(71)	2.475(4)	2.454(4)
Ln(1)−O(51)	2.483(4)	2.460(4)
Ln(1)−O(81)	2.488(4)	2.453(3)
Ln(1)−N(28)	2.509(5)	2.503(4)
Ln(1)−O(61)	2.538(4)	2.488(3)
Ln(1)−N(22A)	2.539(5)	2.488(4)
Ln(1)−O(32)	2.545(4)	2.521(4)
Ln(1)−O(33)	2.604(4)	2.580(4)

Conclusions

The complex anions $[Ru(CN)_4(bpym)]^{2-}$ and $[\{Ru(CN)_4\}_2(\mu\text{-bpym})]$,$^{4-}$ with four and eight externally directed cyanide groups, respectively, crystallize with lanthanide cations to form a range of coordination networks based on Ru−CN−Ln linkages whose structures vary according to the size of the lanthanide cation. These complex anions have lower ^{3}MLCT excited states and shorter emission lifetimes than those of $[Ru(bipy)(CN)_4]^{2-}$ but, nonetheless, show a fast energy transfer to Yb(III), Nd(III), and Er(III), resulting in sensitized near-infrared emissions from these metals. With Yb(III) and Er(III) as energy acceptors, it is clear that the lower energy of the Ru-based ^{3}MLCT states compared to that of $[Ru(bipy)(CN)_4]^{2-}$ is a benefit, because it results in a better energetic overlap with the low-energy f−f states on

Table 7. Selected Bond Distances for the Structures $[\{Ru(CN)_4\}_2(\mu\text{-bpym})][Ln(H_2O)_6]_{0.5}[Ln(H_2O)_4](NO_3)_{0.5}\cdot nH_2O$ (Ln = Eu and Gd and n = 8.5; Ln = Yb and n = 8)

Ru(3)−C(33)	1.969(6)	Ru(3)−C(33)	1.953(6)	Ru(1)−C(33)	1.982(5)
Ru(3)−C(35)	1.985(6)	Ru(3)−C(35)	1.982(6)	Ru(1)−C(35)	1.974(5)
Ru(3)−C(37)	2.025(6)	Ru(3)−C(37)	2.022(6)	Ru(1)−C(37)	2.028(5)
Ru(3)−C(31)	2.056(6)	Ru(3)−C(31)	2.045(6)	Ru(1)−C(31)	2.044(5)
Ru(3)−N(26)	2.101(4)	Ru(3)−N(26)	2.105(4)	Ru(1)−N(12)	2.118(4)
Ru(3)−N(16)	2.128(4)	Ru(3)−N(16)	2.127(4)	Ru(1)−N(22)	2.130(4)
Ru(4)−C(45)	1.978(5)	Ru(4)−C(45)	1.973(5)	Ru(2)−C(63)	1.968(5)
Ru(4)−C(43)	1.978(6)	Ru(4)−C(43)	1.970(6)	Ru(2)−C(65)	1.995(5)
Ru(4)−C(41)	2.017(6)	Ru(4)−C(41)	2.020(6)	Ru(2)−C(61)	2.033(5)
Ru(4)−C(47)	2.041(6)	Ru(4)−C(47)	2.039(6)	Ru(2)−C(67)	2.046(5)
Ru(4)−N(12)	2.123(5)	Ru(4)−N(12)	2.127(5)	Ru(2)−N(51)	2.106(4)
Ru(4)−N(22)	2.132(4)	Ru(4)−N(22)	2.127(4)	Ru(2)−N(41)	2.128(4)
Eu(1)−O(11)	2.470(4)	Gd(1)−O(11)	2.461(4)	Yb(1)−O(11)	2.405(3)
Eu(1)−O(12)	2.453(9)	Gd(1)−O(12)	2.435(5)	Yb(1)−O(12)	2.353(5)
Eu(1)−O(12′)	2.389(9)	Gd(1)−O(13)	2.467(9)	Yb(1)−O(13)	2.266(8)
Eu(1)−O(13)	2.435(6)	Gd(1)−O(13′)	2.366(9)	Yb(1)−O(13′)	2.446(7)
Eu(1)−O(14A)	2.430(8)	Gd(1)−O(14)	2.314(13)	Yb(1)−O(14)	2.378(7)
		Gd(1)−O(14′)	2.524(8)	Yb(1)−O(14′)	2.320(8)
Eu(1)−N(34)	2.446(5)	Gd(1)−N(34)	2.437(5)	Yb(1)−N(38)	2.374(5)
Eu(1)−N(36B)	2.448(6)	Gd(1)−N(36A)	2.433(6)	Yb(1)−N(36)	2.394(5)
Eu(1)−N(42C)	2.458(7)	Gd(1)−N(42B)	2.446(6)	Yb(1)−N(66)	2.359(5)
Eu(1)−N(44)	2.502(7)	Gd(1)−N(44)	2.483(6)	Yb(1)−N(64)	2.360(5)
Eu(2)−O(21)	2.464(5)	Gd(2)−O(21)	2.445(4)	Yb(2)−O(21)	2.314(4)
Eu(2)−O(22)	2.401(4)	Gd(2)−O(22)	2.392(4)	Yb(2)−O(22)	2.325(4)
Eu(2)−O(23)	2.410(5)	Gd(2)−O(23)	2.384(5)	Yb(2)−O(23)	2.357(4)
Eu(2)−N(46)	2.473(5)	Gd(2)−N(46)	2.466(5)	Yb(2)−N(34)	2.400(4)

those lanthanides which act as energy acceptors, despite the lower energy content of the ^{3}MLCT states. The Ru → Ln energy transfer is therefore faster than that in related coordination networks based on $[Ru(bipy)(CN)_4]^{2-}$ as the light-harvesting energy donor.

Experimental Section

Instrumentation and Spectroscopic Methods. FT-IR spectra were recorded on a Perkin-Elmer Paragon instrument using an attenuated total reflection (ATR) accessory, which allowed the spectra of the solids to be determined directly without the need to prepare KBr pellets. UV/vis spectra were recorded on a Cary-50 spectrophotometer. Steady-state luminescence spectra were measured on a Perkin-Elmer LS-50 fluorimeter fitted with a front surface accessory. The instruments, methodology, and data analysis protocols used for the time-resolved luminescence measurements on the near-IR region have been described in detail in previous papers.[5,17]

Syntheses. $K_2[Ru(bpym)(CN)_4]$ and $K_4[\{Ru(CN)_4\}_2(\mu\text{-bpym})]$ were prepared according to the recently described methods.[6,7]

Lanthanide adducts of $[Ru(bpym)(CN)_4]^{2-}$ were prepared as follows. Solutions of $K_2[Ru(bpym)(CN)_4]\cdot 3H_2O$ (0.02 g, 40 μmol) in D_2O (1 cm^3) and the appropriate $Ln(NO_3)\cdot 6H_2O$ (0.2 mmol) in water (2 cm^3) were mixed to give, in all cases, a deep-orange solution, which was stirred for 10 min. Slow evaporation of the resulting solutions over a period of 2−3 weeks resulted in a crop of deep-orange crystals in yields of up to 70%; these were filtered off and washed with methanol and dried under a vacuum. Characterization data are collected in Table 2.

Lanthanide adducts of $[\{Ru(CN)_4\}_2(\mu\text{-bpym})]^{4-}$ were prepared as follows. Solutions of $K_4[\{Ru(CN)_4\}_2(\mu\text{-bpym})]$ (0.015 g, 23 μmol) in D_2O (1 cm^3) and the appropriate $Ln(NO_3)\cdot 6H_2O$ (0.2 mmol) in water (2 cm^3) were mixed to give, in all cases, a deep-red solution, which was stirred for 10 min. Slow evaporation of the resulting solutions over a period of 2−3 weeks resulted in a crop of deep-red crystals in yields of up to 60%; these were filtered off and washed with methanol and dried under a vacuum. Characterization data are collected in Table 2.

X-ray Crystallography. Suitable crystals were mounted on either a Bruker SMART-1000 or a Bruker APEX-2 diffractometer equipped with graphite-monochromatized Mo Kα radiation. Details of the crystal, data collection, and refinement parameters are summarized in Table 3, and selected structural parameters are collected in Tables 4−7. After integration of the raw data and a merging of equivalent reflections, an empirical absorption correction was applied on the basis of a comparison of multiple symmetry-equivalent measurements.[18] The structures were solved by direct methods and refined by full-matrix least squares on weighted F^2 values for all of the reflections using the SHELX suite of programs.[19] None of the refinements presented any significant problems. For coordinated and lattice water molecules, H atoms were added only when both of them showed up clearly in a refinement using only low-angle data; they were then fixed in position with O−H distances of 0.85 Å.

Acknowledgment. We thank the Spanish Ministry of Education and Science for a postdoctoral grant (to J.-M.H.) and the EPSRC (U. K.) for a postdoctoral grant (to S.J.A.P.). We also thank Johnson Matthey for the loan of some potassium hexacyanoruthenate.

Supporting Information Available: Crystallographic files of complexes in this study in CIF format. This material is available free of charge via the Internet at http://pubs.acs.org.

IC0521574

(17) Beeby, A.; Faulkner, S. *Chem. Phys. Lett.* **1997**, *266*, 116.

(18) Sheldrick, G. M. *SADABS*: *A Program for Absorption Correction with the Siemens SMART System*; University of Gottingen: Gottingen, Germany, 1996.

(19) *SHELXTL Program System*, version 5.1; Bruker Analytical X-ray Instruments Inc.: Madison, WI, 1998.